Asia-Pacific Journal of Science and Technology :Volume :xx Issue :xx Article ID :APST-xx-xx-xx Research Article

APST

Asia-Pacific Journal of Science and Technology

https//:www.tci-thaijo.org/index.php/APST/index

Published by Research and Innovation Department,
Khon Kaen University, Thailand

# Electro-oxidation of glycerol on CoNiBi supported on carbon cloth in alkaline media

Wasu Chaitree[1*], Boorata Dechpisutthithum[1], Winrath Khrutchan[1], Muthita Kongroiyou[1], Chiwathan Srimangkorn[1], Ratthammanoon Sakulsinghdusit[1], and Joongjai Panpranot[2]

[1]Department of Chemical Engineering, Faculty of Engineering and Industrial Technology, Silpakorn University, Nakhon Pathom 73000, Thailand
[2]Center of Excellence on Catalysis and Catalytic Reaction Engineering, Department of Chemical Engineering, Faculty of Engineering, Chulalongkorn University, Bangkok 10330, Thailand
[*]Corresponding author: chaitree_w@su.ac.th

Received 15 August 2025
Revised 14 November 2025
Accepted 21 December 2025

**Abstract**

Toward the development of non-noble metal electrocatalysts for the valorization of glycerol, the effect of the addition of Bi on Co-Ni electrocatalysts supported on carbon cloth (CC) for the electro-oxidation of glycerol (EOG) was investigated. The CoNiBi/CC electrocatalysts were prepared via an electroless deposition method and characterized using X-ray diffraction, scanning electron microscopy, energy-dispersive X-ray spectroscopy, and X-ray photoelectron spectroscopy. Their electrochemical activity was investigated using cyclic voltammetry, linear sweep voltammetry, and chronoamperometry. The effect of the Bi $(NO_3)_3$ concentration in the electroless bath on the EOG performance was studied, finding that CoNiBi/CC prepared using 6 mM Bi $(NO_3)_3$ (CoNiBi_6/CC) provided higher current density and lower onset potential than other electrocatalysts. The effect of applied potentials on the formation of products was also investigated. The analysis of the liquid products using high-performance liquid chromatography showed that formic acid (FA) was obtained as the main product along with oxalic acid as a minor product. The highest rate of FA formation was 772.95 μmol $cm^{-2}$ $h^{-1}$ at 0.7 V vs. Ag/AgCl after 2 h of reaction, and the highest selectivity for FA was 77.5% at 0.6 V vs. Ag/AgCl. Overall, the CoNiBi/CC electrocatalyst is a promising and cost-effective alternative for the electrochemical valorization of glycerol into value-added chemicals.

**Keywords:** Bismuth, Cobalt, Electro-oxidation of glycerol, Nickel

## 1. Introduction

The continuously increasing global energy demand has led to an excessive consumption of fossil fuels, resulting in massive greenhouse gas emissions, particularly $CO_2$, which cause global climate change, environmental degradation, and rising sea levels. Consequently, the development and adoption of renewable and sustainable energy sources is critical for reducing fossil fuel consumption and meeting the energy demands. In this context, the expansion of the biodiesel industry has led to a surplus of glycerol ($C_3H_8O_3$), a byproduct of biodiesel production, prompting intense research into its conversion into high-value-added products [1, 2]. In particular, the electro-oxidation of glycerol (EOG) in an alkaline electrolyte has emerged as a promising approach for the valorization of glycerol into useful intermediates, including glycolate, glycerate, tartrate, hydroxy pyruvate, glycolic acid, oxalic acid, oxalate, dihydroxyacetone, and formate ions [3].

The EOG requires a high-efficiency anode material. Research into EOG has consistently highlighted the critical dependence of the reaction kinetics on the properties of the anode electrocatalyst. While platinum (Pt) is traditionally employed in EOG due to its superior intrinsic activity, its widespread implementation is constrained by prohibitive material costs. Furthermore, Pt-based electrocatalysts are highly susceptible to performance degradation caused by surface poisoning from intermediate species, particularly carbon monoxide (CO) or aldehydic (CHO) species. Therefore, transition metals, including Ni and Co, are widely used as active surface

sites for the EOG. However, individual metallic components often result in a slow rate of reaction. the design of multi-metallic compositions facilitates the emergence of enhanced physicochemical properties when compared to the corresponding individual metallic components.

Moreover, the combination of both transition metals as an electrocatalyst (Ni–Co) for diverse reactions offers a cost-effective alternative to noble metals like Ag, Pt, and Pd. In addition to their low cost, Ni and Co have multiple oxidation states, rendering them suitable for various catalytic reactions, particularly oxidation–reduction reactions involving electron transfer [4]. For instance, Biuck H. and Nasrin D. [5] used Ni-Cu and Ni–Co nanoparticles supported on carbon ceramic electrodes for the EOG in alkaline media, finding that Ni-Cu and Ni–Co delivered higher current densities than pure Ni. In addition, to improve their catalytic performance, Ni- and Co-based electrocatalysts have been modified by a third metal. For example, Mohamed S. E. Houache et al. [6] reported that the combination of Ni and Bi exhibited enhanced electrochemical performance in the EOG in terms of enhanced oxidation–reduction reactions, faster reaction rates, and greater stability compared with monometallic Ni, demonstrating that the incorporation of Bi boosted the performance of the Ni electrocatalyst.

In this work, an electroless deposition method was used to prepare CoNiBi electrocatalysts supported on carbon cloth (CC). The electrocatalysts were characterized using X-ray diffraction (XRD), energy-dispersive X-ray spectroscopy (EDX), scanning electron microscopy (SEM), and X-ray photoelectron spectroscopy (XPS). The EOG was conducted in a H-cell reactor, and the effects of the Bi $(NO_3)_3$ concentration in the electroless bath and the applied potentials on the EOG performance were investigated.

## 2. Materials and methods

### *2.1 Chemicals*

All chemicals used for the preparation of the electrocatalysts are summarized in Table 1. Electroless baths were prepared by dissolving the corresponding chemicals in deionized (DI) water, making up a total volume of 250 mL.

**Table 1** Chemicals used as precursors catalyst preparation.

| Chemicals | Concentration (mol/L) |
|---|---|
| Cobalt (II) sulfate heptahydrate (Sigma-Aldrich) | 0.0249 |
| Nickel (II) sulfate hexahydrate (Sigma-Aldrich) | 0.0266 |
| Sodium borohydride (Q RëC) | 1 % wt in 10 ml |
| Ethylenediaminetetraacetic acid (EDTA) (Sigma-Aldrich) | 0.0206 |
| Potassium Sodium tartrate tetrahydrate (Sigma-Aldrich) | 0.0354 |
| Potassium D-gluconate (Alfa Aesar) | 0.0218 |
| Boric Acid (Kemaus) | 0.0808 |
| Sodium citrate dihydrate (Sigma-Aldrich) | 0.0340 |
| Bi (III) Nitrate heptahydrate (Kemaus) | 0.003 ,0.06 ,0.09 ,0.012 |

### *2.2 Preparation of Pd–polymer ink*

Palladium acetate (Tokyo Chemical Industry) 0.098g was mixed with 2 mL of ammonium hydroxide (Sigma-Aldrich) while slowly stirring at 30°C until complete dissolution of palladium acetate. Next, polyvinyl butyral (Butvar B-98, Eastman Chemical) 22 g was dissolved in methanol (140 mL, Sigma-Aldrich) with continuous mixing and vigorous shaking to reach homogeneity. Then, the first mixture was poured into the second one and the final mixture was stirred for approximately 20 h until thoroughly mixed.

### *2.3 Preparation of catalyzed CC*

A CC with dimensions of $5 \times 5$ $cm^3$ (purchased from Fuel Cell Earth) was cut and coated with the Pd–polymer ink. For coating process, approximately 5ml of the Pd-polymer ink was applied uniformly to both sides of the carbon cloth. After that, the coated substrate was dried for at least 2–3 h. Then, the coated CC was annealed at 375 °C for 20 h, and the resulting catalyzed CC was used as a support.

*2.4 Preparation of CoNiB_x/CC electrocatalysts*

The electroless plating of CoNiBi was conducted at 75°C±5°C and a pH of 10±1. 0.5 M NaOH was used to adjust pH. CC was cut and immersed in the electroless bath for 30 min, and 1 wt.% $NaBH_4$ was added dropwise to the homogenous mixture for the precipitation–reduction to occur. After plating, the substrate was rinsed with DI water and methanol. Finally, the as-prepared electrocatalyst was dried at 60°C. The obtained electrocatalysts were labeled as CoNiBi x/CC (x = 3, 6, 9, and 12 mM), where x is the concentration of Bi $(NO_3)_3 \cdot 5H_2O$ in the electroless bath. For the electroless plating of CoNi/CC, the same procedure was used.

*2.5 Electrochemical measurements*

All electrochemical measurements were performed using a potentiostat/galvanostat in a conventional three-electrode system consisting of a Pt wire as the counter electrode, Ag/AgCl (saturated KCl) as the reference electrode, and CoNiBi_x/CC as the working electrode. The electrochemical behavior and electrocatalytic performance in the EOG were investigated by performing cyclic voltammetry (CV), LSV, and chronoamperometry (CA) measurements in an aqueous electrolyte solution of 0.5 M KOH with 1 M glycerol. The CV measurements were performed at a scan rate 20 mV $s^{-1}$ in a potential range from −1.0 to 1.0 V vs. Ag/AgCl. The LSV curves were recorded at 1 mV $s^{-1}$ and between −0.7 and 0.7 V vs. Ag/AgCl. CA was conducted at a constant potential of 0.2 V vs. Ag/AgCl for 2 h.

*2.6 EOG in a H-cell*

The anode and cathode compartments were separated using an anion exchange membrane (Fuel Cell Earth, Fumasep FAA-3-PK-130). The anodic site contained the working electrode (CoNiBi_x/CC) and the reference electrode (Ag/AgCl). The cathodic site contained Pt foil (1.5 $cm^2$). The anolyte and catholyte were 0.5 M KOH + 1 M glycerol and 2 M KOH, respectively. The geometric area of the electrocatalyst was 1 × 1 $cm^2$. After a reaction time of 2 h, 0.5 mL of sample was collected from the electrochemical cell and mixed with 0.5 mL of 0.25 M $H_2SO_4$, and the mixed solution was put in vials. The liquid products were analyzed via high-performance liquid chromatography (HPLC). The product selectivity and the conversion were calculated according to the following formula (Equation 1 and Equation 2):

$$\text{Selectivity (\%)} = \frac{concentration\ of\ the\ specific\ product}{Total\ concentration\ of\ all\ product} \text{ x } 100 \quad (1)$$

$$\text{Conversion (\%)} = \frac{Initial\ concentration\ of\ glycerol - Final\ concentration\ of\ glycerol}{Initial\ concentration\ of\ glycerol} \text{ x } 100 \quad (2)$$

**3. Results and discussion**

*3.1 SEM, EDX, XRD, and XPS results*

The SEM images of CC, CoNiBi_x/CC, and CoNi/CC are illustrated in Figure 1(A)–(F). As shown in Figure 1A, CC exhibited a cylindrical and porous structure. After the electroless deposition, the SEM images of CoNiBi_3/CC (Figure 1B), CoNiBi_6/CC (Figure 1C), CoNiBi_9/CC (Figure 1D), and CoNiBi_12/CC (Figure 1E) showed that metal particles with a somewhat spherical shape were deposited on CC thin films. In contrast, an irregular particle shape was observed for CoNi/CC (Figure 1F). This can be attributed to the lack of $Bi^{3+}$ in the electroless bath, which is known to act as a stabilizer to prevent an excessively fast deposition rate resulting in the formation of irregular particles [7].

Table 2 shows the EDX-determined atomic percentage (%At) of C, Co, Ni, and Bi. The %At of Bi element increased with increasing Bi $(NO_3)_3$ concentration in the electroless bath. Moreover, the %At of Co was higher than that of Ni across all samples, consistent with anomalous codeposition occurred during the electrolytic deposition [8]. Typically, in the Co-Ni alloy deposition, Co is less noble metal compared to Ni, which results in Co being deposited preferentially over Ni, even when the Ni concentration is higher in the bath. Furthermore, the %At of Co in the CoNi/CC was approximately twice that of Ni. The specific reason for this degree of preference remained unclear for the CoNi/CC result. However, it is hypothesized that $Bi^{3+}$ acts as a kinetic control agent or stabilizer. Its adsorption onto the substrate may partially inhibit the preferential deposition of Co-the less noble metal- thereby pushing the Co:Ni ratio closer to the expected ratio from the bulk solution. Without $Bi^{3+}$, this inhibition is absent, allowing Co to deposit with a much higher preference.

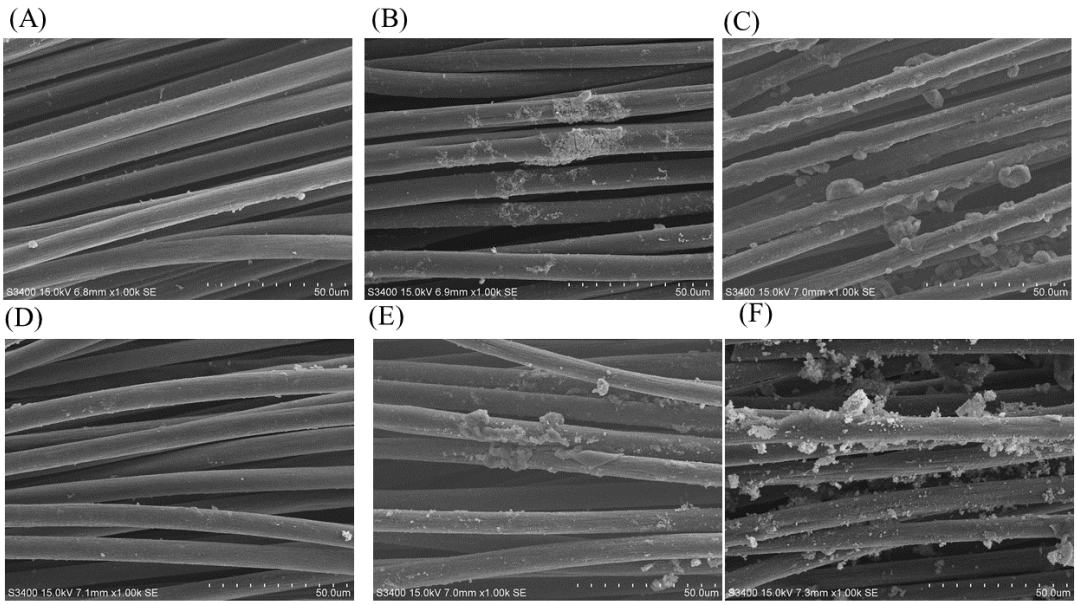


**Figure 1** SEM images: (A) CC, (B) CoNiBi 3/CC, (C) CoNiBi_6/CC, (D) CoNiBi_9/CC, (E) CoNiBi_12/CC, and (F) CoNi/CC captured at 1 k magnifications.

**Table 2** Atomic percentage (%At) of C, Co, Ni, and Bi by EDX analysis.

| Electrocatalysts | Atom (%) | | | |
|---|---|---|---|---|
| | C | Ni | Co | Bi |
| CoNiBi_3/CC | 98.68 | 0.60 | 0.65 | 0.07 |
| CoNiBi_6/CC | 98.39 | 0.71 | 0.73 | 0.17 |
| CoNiBi_9/CC | 98.15 | 0.79 | 0.81 | 0.25 |
| CoNiBi_12/CC | 97.86 | 1.11 | 1.15 | 1.13 |
| CoNi/CC | 90.02 | 3.16 | 6.82 | NA |

Figure 2 shows the XRD patterns of CoNiBi_x/CC and CoNi/CC, which exhibit reflection peaks at 43.5° and 53.7° attributable to the (111) and (200) crystal planes of CoNi, respectively, indicating the presence of CoNi in the electrocatalysts. In addition, the XRD patterns of CoNiBi_x/CC show peaks at 26.8° corresponding to the (201) crystal plane of $Bi_2O_3$, at 35.3° and 31.8° for the (202) crystal plane of $Bi_2O_3$, and at 31.7° for the (212) crystal plane of $Bi_2O_3$. As the Bi $(NO_3)_3$ concentration in the electroless bath increased, the peaks corresponding to Bi species at 26.8° and 35.3° were more clearly observed.

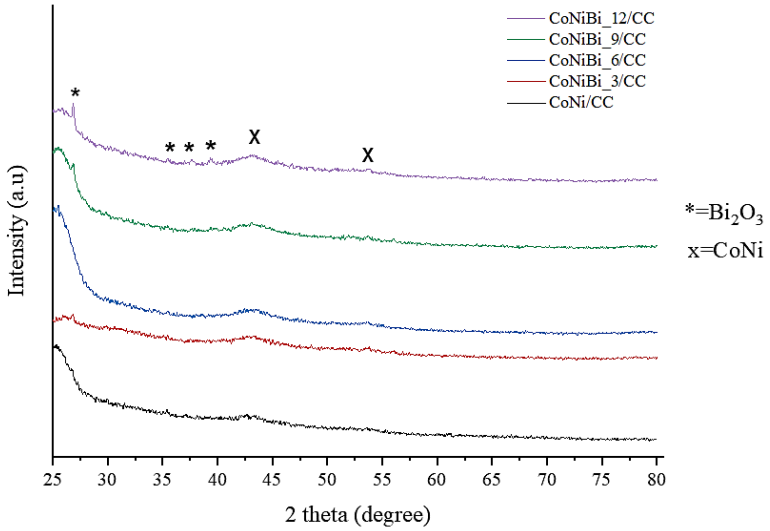


**Figure 2** XRD patterns of CoNiBi_x/CC and CoNi/CC**.**

The chemical bonding states of Co 2p, Ni 2p, and Bi 4f for CoNiBi_X/CC were analyzed using XPS (Figures S1–S4 and Table 3). In the Co 2p XPS spectra, the peaks at 871.7–873.1 and 796.3–798.7 eV can be assigned to $Co^{2+}$ [9, 10]. Meanwhile, the peaks located at 854.3–856.1 and 874.3–878.6 eV in the Ni 2p XPS spectra are attributable to $Ni^{2+}$ [9, 11, 12]. In the Bi 4f XPS spectra, the peaks detected at 158.2–160.1 and 163.5–165.4 eV correspond to $Bi^{3+}$ [13], revealing the presence of Bi species in agreement with the XRD results. The presence of $Co^{2+}$, $Ni^{2+}$, and $Bi^{3+}$ in the XPS spectra suggests that Co–Ni–Bi underwent partial oxidation.

**Table 3** Chemical bonding states of (a) Co 2*p* Ni 2*p* Bi *4f* on CoNiBi_X/CC.

| Electrocatalysts | Binding Energy (eV) | Chemical states | Binding Energy (eV) | Chemical states | Binding Energy (eV) | Chemical states |
|---|---|---|---|---|---|---|
| | Co *2p* | | Ni *2p* | | Bi *4f* | |
| CoNiBi_3/CC | 781.7 | $Co^{2+}$ | 855.4 | $Ni^{2+}$ | 158.2 | $Bi^{3+}$ |
| | 796.3 | $Co^{2+}$ | 874.0 | $Ni^{2+}$ | 163.5 | $Bi^{3+}$ |
| CoNiBi_6/CC | 782.4 | $Co^{2+}$ | 856.1 | $Ni^{2+}$ | 160.1 | $Bi^{3+}$ |
| | 797.6 | $Co^{2+}$ | 874.6 | $Ni^{2+}$ | 165.4 | $Bi^{3+}$ |
| CoNiBi_9/CC | 783.1 | $Co^{2+}$ | 854.3 | $Ni^{2+}$ | 159.8 | $Bi^{3+}$ |
| | 797.3 | $Co^{2+}$ | 875.6 | $Ni^{2+}$ | 165.2 | $Bi^{3+}$ |
| CoNiBi_12/CC | 782.4 | $Co^{2+}$ | 855.6 | $Ni^{2+}$ | 159.3 | $Bi^{3+}$ |
| | 798.7 | $Co^{2+}$ | 873.3 | $Ni^{2+}$ | 164.6 | $Bi^{3+}$ |

*3.2 LSV, CV, and CA results*

Figures 3(A)–(D) displays the LSV curves of CoNiBi_X/CC in KOH in the absence and presence of glycerol. An increase in current density was observed in the EOG (red line) for all electrodes compared with the system without glycerol (water splitting, black line). Moreover, the onset potential for the EOG was lower than that for the water splitting, indicating that the former reaction was kinetically and thermodynamically favored over the oxygen evolution reaction in water splitting. The peaks around 0.4 V vs. Ag/AgCl in the water splitting curves for all electrodes probably stemmed from the oxidation of deposited metals [14]. Figure 4A shows the LSV curves of CoNiBi_X/CC, CoNi/CC, and CC in the EOG. For CoNiBi_x/CC, the highest current density was observed on CoNiBi_6/CC ($0.048$ A $cm^{-2}$ at 0.7 V vs. Ag/AgCl), indicating that this electrode was the most effective for the reaction. In addition, CoNiBi_6/CC delivered higher current density and lower onset potential than CoNi/CC, indicating that Bi enhanced the reaction performance. Generally, the reaction rate is proportional to the current density, as dictated by Faraday's law of electrolysis. Consequently, the high current density corresponds to a faster reaction rate. Furthermore, the onset potential is defined as the minimum voltage at which an electrochemical reaction begins to occur. Therefore, a lower onset potential signifies that the reaction can be initiated more easily.

Conversely, CC showed the lowest current density for the EOG. Typically, Pd is an effective electrocatalyst for the EOG. However, in this study, Pd was used as an initiation point for the electroless deposition and was covered by Co, Ni, or Bi, hindering its participation in the reaction.

To further justify and support the deduction made about the role of bismuth, we performed a preliminary investigation to determine the reaction rate constant values ($k$, Equation 3-4) and activation energies ($E_a$, Equation 5) of CoNiBi_6/CC and CoNi/CC [15]. It is noted that the reaction rate is proportional to the current density, as established by Faraday's law of electrolysis.

$$rate = i = kC^n \tag{3}$$

$$\ln i = \ln k + n \ln C \tag{4}$$

$$E_a = -R\left[\frac{d\ln(i)}{d\left(\frac{1}{T}\right)}\right] \tag{5}$$

In Equation (3), $i$ is the peak current density (A/$cm^2$), $k$ is the reaction rate constant, $C$ is the bulk concentration and $n$ is the reaction order. In Equation (5), $T$ is the reaction temperature (K), $R$ is the gas constant. In this study, glycerol concentrations were varied from 0.2-1 M and temperatures were varied from 30-60 °C (Figure S4). Table 4 summarized the determined activation energy and the rate constant values. The result indicated that $E_a$ for CoNiBi_6/CC was lower than that of CoNi/CC. Additionally, the rate constant value for the CoNiBi_6/CC was

found to be higher than the CoNi/CC. The lower activation energy and the higher reaction rate constant of CoNiBi_6/CC electrode strongly suggests that the modification of Bi makes a beneficial contribution for EOG.

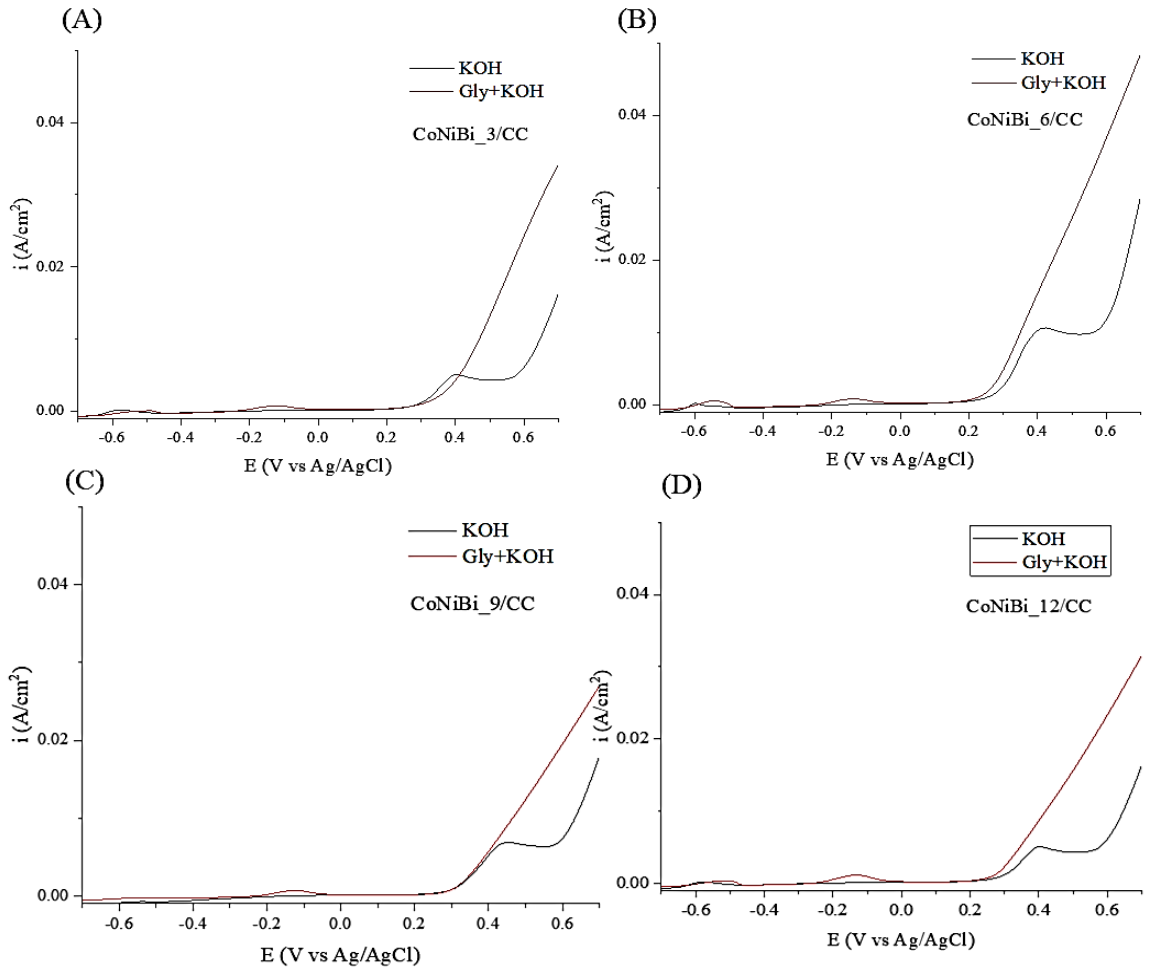


**Figure 3** LSV curves of CoNiBi_X/CC in KOH with the absence and the presence of glycerol. (A) CoNiBi_3/CC, (B) CoNiBi_6/CC, (C) CoNiBi_9/CC, and (D) CoNiBi_12/CC. (Gly=glycerol).

**Table 4** Activation energies and rate constant values for two electrodes.

| Electrocatalysts | $E_a$ (kJ/mol) | k ($L \cdot mol^{-1} \cdot s^{-1}$) |
|---|---|---|
| CoNiBi_6/CC | 33.1 | 0.0028 |
| CoNi/CC | 27.8 | 0.0018 |

On the basis of the above results, CoNiBi_6/CC was selected for the CV studies (Figure 4B). The formations of oxide, hydroxide, or oxyhydroxide groups, which served as the active sites in the oxidation of alcohol were indicated at −0.5 V vs. Ag/AgCl (Peak $A_1$) [16, 17]. Additionally, XRD patterns of CoNiBi_6/CC after the CV test (Figure 4C) showed the peaks at 35.5° and 53.0 °corresponding to the formation of the Ni-Co oxyhydroxide group [18]. However, the XRD technique is difficult to distinguish Ni and/or Co oxyhydroxide probably because their peaks overlap each other and take place at almost the same diffraction angles [19].

Then, the EOG was observed in the forward scan at −0.09 V vs. Ag/AgCl (Peak $A_2$). Typically, the formation of chemicals including, dihydroxyacetone, glyceraldehyde, glycolic acid, oxalic acid, and formic acid is indicated at the oxidation peak in the forward scan [20, 21]. Meanwhile, Peak $A_3$ in the backward scan can be attributed to the reduction of metal oxide, metal hydroxide, or metal oxyhydroxide to metals. Finally, Peak $A_4$ probably corresponds to the formation of the final product (CO or $CO_2$) [22].

The CA results (Figure 5A and B) showed that CoNiBi_X/CC exhibited high stability and durability. CoNiBi_3/CC, CoNiBi_6/CC, CoNiBi_9/CC, and CoNiBi_12/CC delivered current densities of 0.436, 0.724,

0.723, and 0.709 mA $cm^{-2}$, respectively at 7200 s, suggesting that the Bi $(NO_3)_3$ concentration did not considerably affect the stability of the electrocatalysts. Furthermore, the current density substantially decreased within 0–50 s, possibly due to poisoning of the electrocatalyst surface. The current densities of CoNiBi_X/CC were relatively higher than that of CuNi/CC (Figure 5B), suggesting that Bi enhanced the electrode stability. Recently, multimetallic electrodes have been shown to exhibit higher stability than those with monometallic compositions. For instance, Wang et al. [23] revealed that a PdBi electrocatalyst delivered higher current density (0.28 A $g_{Pd}^{-1}$) than Pd (0.026 A $g_{Pd}^{-1}$) for the EOG at 3600 s. Moreover, Houache et al. [24] reported that a NiBi electrocatalyst was more stable than pure Ni.

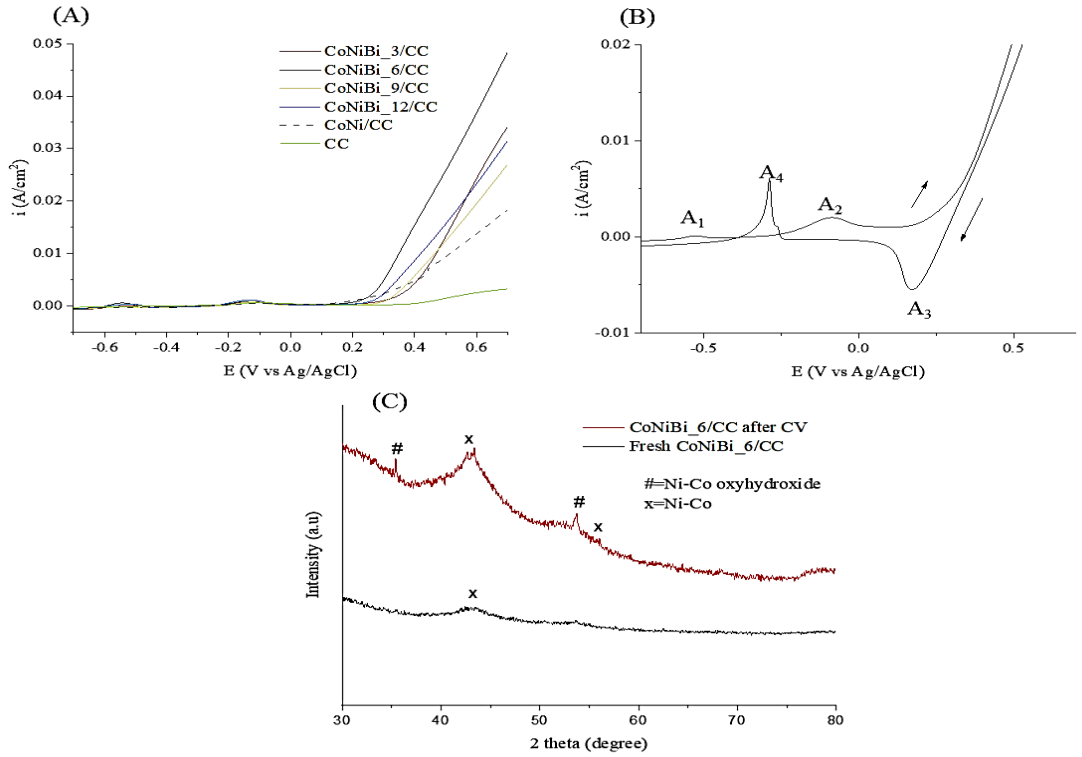


**Figure 4** (A) LSV curves of CoNiBi_X/CC, CoNi/CC, and CC in KOH+glycerol (B) CV curve of CoNiBi_6/CC in KOH+glycerol (C) XRD patterns of fresh CoNiBi_6/CC and CoNiBi_6/CC after CV.

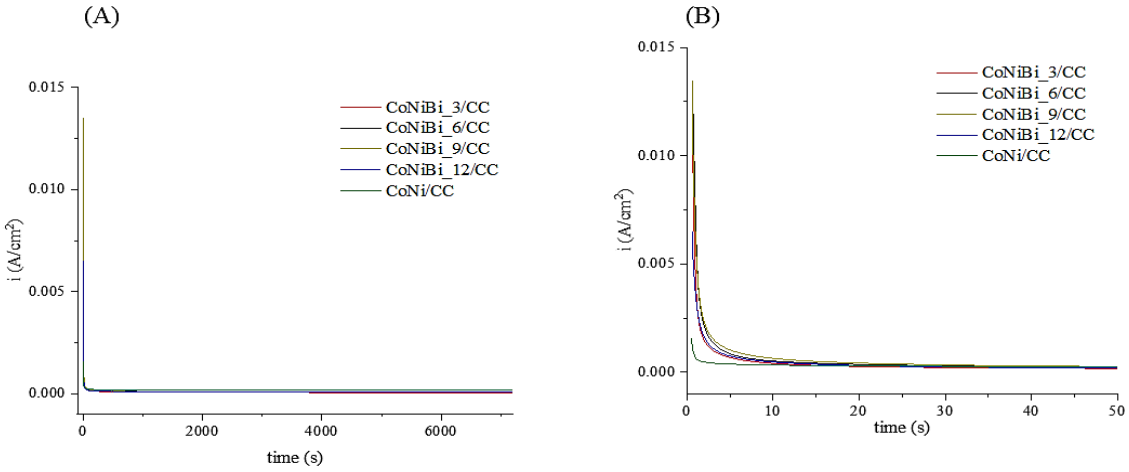


**Figure 5** CA curves of CoNiBi_X/CC and CoNi/CC in EOG for (A) 7200s, (B) 50s.

*3.3 Liquid products from the EOG on CoNiBi_6/CC*

Table 5 shows the rates of formation of liquid products detected by HPLC (a representative HPLC spectrum is shown in Figure S6), which were oxalic acid (OA), FA, and glycolic acid (GA). FA was the main product in all applied potentials (0.5–0.8 V vs. Ag/AgCl). At 0.5 and 0.6 V vs. Ag/AgCl, the main product was FA and the

minor product was OA, whereas GA was not observed. Upon increasing potential to 0.7 V vs. Ag/AgCl, a change in the product distribution was observed. A marked increase in FA production was observed, along with a noticeable formation of GA, whereas the amount of OA remained nearly constant. However, at 0.8 V vs. Ag/AgCl, the rate of formation of FA slightly decreased and that of GA tended to increase. These results indicate that the formation of FA and OA was dependent on the applied potential. Specifically, FA and OA were formed at high potentials, but at 0.8 V vs. Ag/AgCl, FA was probably converted to $CO_2$ or CO, thereby decreasing its formation rate [25]. The reason for the formation of GA at high potentials remains unclear, although it could be directly formed from glyceric acid [26]. As shown in Figure 6, at all applied potentials (0.5–0.8 V vs. Ag/AgCl), the highest rate of FA formation was 772.95 μmol $cm^{-2}$ $h^{-1}$ at 0.7 V vs. Ag/AgCl after 2 h of reaction, but the highest selectivity for FA was 77.5% at 0.6 V vs. Ag/AgCl, which was higher than for other products. Additionally, the conversion of glycerol slightly increased with increasing the applied potentials from 61.3% (at 0.5 V) to 68.7% (at 0.8 V). This trend reflected the higher driving force for the electrochemical reaction as the potential increased, resulting in greater oxidative activation of glycerol. Significantly, the onset of GA formation at 0.7 V (with a rate of 399.0 μmol/$cm^2$.h) and the significant increase in the FA rate from 409.1 to 772.9 μmol/$cm^2$.h at 0.7 V indicate that the higher applied potential activates different reaction pathways, leading to the production of multiple valuable products.

SEM was used to investigate the morphology changes of CoNiBi_6/CC after the EOG at 0.5–0.8 V vs. Ag/AgCl (Figure 7A–E). A comparison of the SEM images of fresh and spent CoNiBi_6/CC showed that after the EOG, the CC surface was covered with some nonuniform particles that gathered into larger particles probably due to metal particles falling off and then recombining during the electrolysis. Therefore, CoNiBi/CC exhibited high stability and strong resistance to the EOG conditions. Additionally, Table 6 shows the EDX-determined atomic percentage (%At) of C, Co, Ni, and Bi for the spent CoNiBi_6/CC after electrochemical testing at 0.5 V, 0.6 V, 0.7 V, and 0.8 V vs Ag/AgCl, respectively. The result showed that Co, Ni, and Bi were still detected, which confirmed that metals remained on the carbon surface. However, the %At of all metal elements decreased following reaction. A reduction likely resulted from the metal passivation and dissolution processes that occur during the electrochemical reaction. Furthermore, the XRD patterns of the fresh and spent CoNiBi_6/CC after the stability test (CA in Figure 5) are shown in Figure 8. The peaks at 43.5° and 53.7° corresponded to the of Co-Ni composition on CC, suggesting that CoNiBi_6/CC exhibited high structural stability. Additionally, the peaks related to Bi species were not detected on either the fresh or spent electrocatalyst which was attributed to the low atomic percentage of Bi deposited on the surface.

**Table 5** Rates of formation of OA, GA, and FA detected by HPLC.

| E (V vs Ag/AgCl) | Conversion of glycerol (%) | Rate (μmol/$cm^2$.h) | | |
|---|---|---|---|---|
| | | Oxalic acid (OA) | Glycolic acid (GA) | Formic acid (FA) |
| 0.5 V | 61.3 | 119.7 | NA | 355.1 |
| 0.6 V | 62.9 | 119.1 | NA | 409.1 |
| 0.7 V | 65.9 | 130.2 | 399.0 | 772.9 |
| 0.8 V | 68.7 | 139.4 | 452.7 | 586.8 |

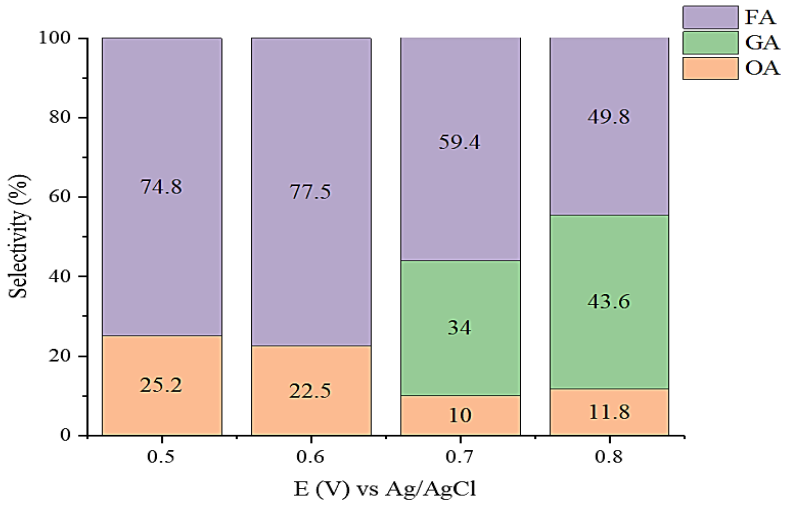


**Figure 6** Percentage of selectivity of FA, GA, and OA based on different applied potentials (reaction time 2 h).

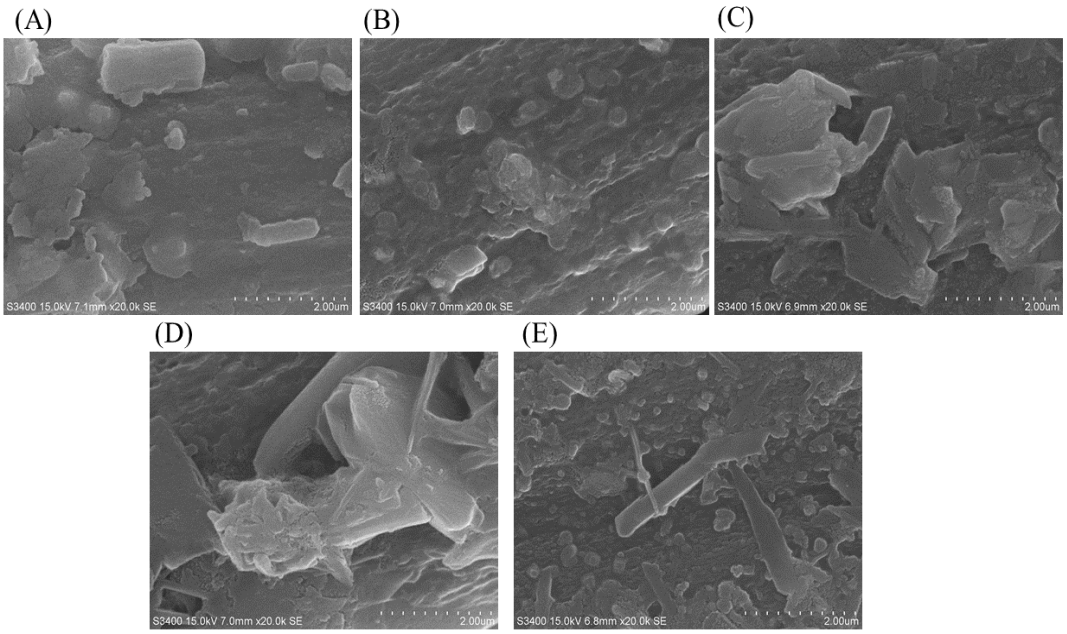


**Figure 7** Morphology images of: (A) fresh CoNiBi_6/CC and spent CoNiBi_6/CC after EOG at (B) 0.5 V, (C) 0.6 V, (D) 0.7 V, and (E) 0.8 V.

**Table 6** Atomic percentage (%At) of C, Co, Ni, and Bi of spent CoNiBi_6/CC by EDX analysis.

| Electrocatalysts | Atom (%) | | | |
|---|---|---|---|---|
| | C | Co | Ni | Bi |
| Fresh CoNiBi_6/CC | 98.39 | 0.71 | 0.73 | 0.17 |
| Spent CoNiBi_6/CC | | | | |
| 0.5 V | 98.50 | 0.68 | 0.69 | 0.14 |
| 0.6 V | 98.73 | 0.50 | 0.67 | 0.10 |
| 0.7 V | 98.87 | 0.46 | 0.59 | 0.08 |
| 0.8 V | 99.06 | 0.33 | 0.55 | 0.06 |

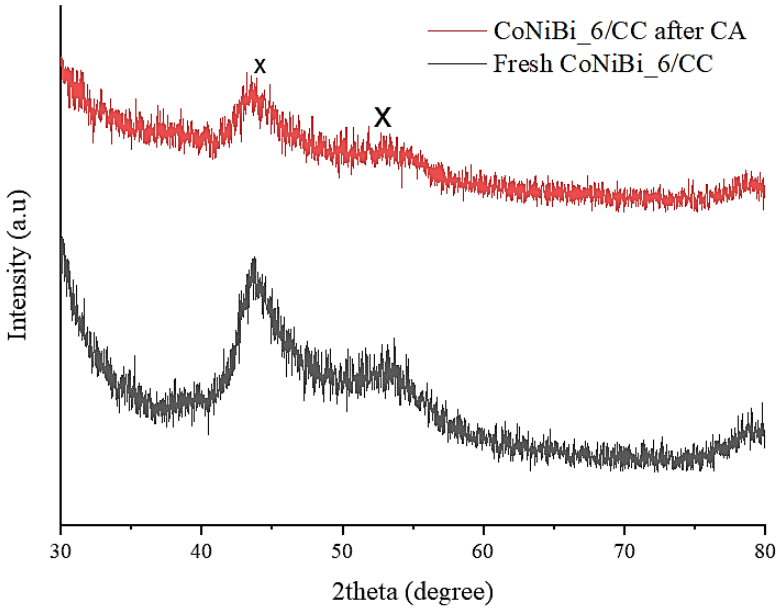


**Figure 8** XRD patterns of spent CoNiBi_6/CC after EOG (x=Co-Ni).

## 4. Conclusions

CoNiBi_x/CC electrocatalysts were successfully synthesized via electroless deposition and used for the EOG. CoNiBi_6/CC exhibited the best performance among the electrocatalyst series, showing the lowest onset potential and the highest current density. The LSV and CA results revealed that Bi helped enhance not only the reaction performance but also the stability of the electrocatalysts. The reaction test in a H-cell reactor showed that glycerol was converted into OA, FA, and GA, with FA being the main product in all applied potentials (0.5–0.8 V vs. Ag/AgCl). The highest rate of FA formation was 772.95 μmol $cm^{-2}$ $h^{-1}$ at 0.7 V vs. Ag/AgCl after 2 h of reaction. However, the highest selectivity for FA (77.5%) was seen at 0.6 V vs. Ag/AgCl because only two products were formed at this potential. Overall, this work underscores the potential of non-noble metal electrocatalysts for the valorization of glycerol.

## 5. Acknowledgements

This research is financially supported by Thailand Science Research and Innovation (TSRI) National Science, Research and Innovation Fund (NSRF) (Fiscal Year 2024). The authors would like to thank the Department of Chemical Engineering, Faculty of Engineering and Industrial Technology, Silpakorn University and Department of Chemical Engineering, Chulalongkorn University.

## 6. Author Contributions

Wasu Chaitree: Conceptualization, Validation, Supervision, Writing - review & editing, Funding acquisition. Boorata Dechpisutthithum, Winrath Khrutchan, Muthita Kongroiyou, Chiwathan Srimangkorn, Ratthammanoon Sakulsinghdusit: Writing - original draft, Investigation. Joongjai Panpranot: Resources, Supervision.

## 7. Conflicts of interest

The authors declare that there is no conflict of interest.

## 8. References

[1] Pagliaro MV, Bruni F, Oberhauser W, Capozzoli L, Berretti E, Bartoli F. Hydrogen and high-value-added chemicals from glycerol electroreforming using a highly efficient and selective ligand-stabilized PdCu catalyst. ACS Sustainable Chem Eng. 2025;13(13):4975–4987.

[2] Sarkar A, Tyagi T, Sharma S, Joshi V, Gogoi P, Puzari A. Synthesis of glycerol carbonate from glycerol and $CO_2$ over Cu/$In_2O_3$/ZnO nanostructured catalyst. Catal Today. 2025;448:115164.

[3] Terekhina I, WhiteAnn J, Johnsson C. Electrocatalytic oxidation of glycerol to value-added compounds on Pd nanocrystals. ACS Appl Nano Mater. 2023;6(13):11211–11220.

[4] Massaneiro J, Valério TL, Pellosi DS, Silva BJGd, Vidotti M. Electrocatalytic oxidation of glycerol performed by nickel/cobalt alloys: Adding value to a common subproduct of chemical industry. Electrochim Acta. 2024;506:145013.

[5] Habibi B, Delnavaz N. Electrooxidation of glycerol on nickel and nickel alloy (Ni-Cu and Ni-Co) nanoparticles in alkaline media. RSC Adv. 2016;6:31797-31806.

[6] Houache MSE, Safari KH, Botton GA, Baranova EA. Modification of nickel surfaces by bismuth: Effect on electrochemical activity and selectivity toward glycerol. ACS Appl Mater Interfaces 2020;12(13):15095–15107.

[7] Wang K, Hong L, Liu Z-L. The role of $Bi^{3+}$ complex ion as the stabilizer in electroless nickel plating process. AIChE J. 2009;55(4):1046-1055.

[8] Domańska AJ, Skitał PM. Electrodeposition of alloy nanostructures (Co-Ni) in the presence of sodium benzene sulfonate (SBS) and their application in alkaline hydrogen evolution. Molecules. 2025;30:1771.

[9] Yin X, Li H, Yuan R, Lu J. Hierarchical self-supporting sugar gourd-shape MOF-derived $NiCo_2O_4$ hollow nanocages@SiC nanowires for high-performance flexible hybrid supercapacitors. J Colloid Interface Sci. 2021;586:219-232.

[10] Afzali N, Keshavarzi R, Tangestaninejad S, Gimenez S, Mirkhani V, Moghadam M. Multifunctional approach to improve water oxidation performance with MOF-based photoelectrodes. Appl Mater Today. 2021;24:2-4.

[11] Yang X, Wang D, Yu R, Bai Y, Shu H, Ge L. Suppressed capacity/voltage fading of highcapacity lithium-rich layered materials via the design of heterogeneous distribution in the composition. J Mater Chem A. 2014;2:3899-3911.

[12] Li Z, Bian C, Hu L. Exploration of the corrosion behavior of electroless plated Ni-P amorphous alloys via x-ray photoelectron spectroscopy. Molecules. 2023;28:377-380.

[13] Singh S, Sahoo RK, Shinde NM, Yun JM, Mane RS, Chung W. Asymmetric faradaic assembly of $Bi_2O_3$ and $MnO_2$ for a high-performance hybrid electrochemical energy storage device. RSC Adv. 2019;9:32154–32164.

[14] Hu E, Yao Y, Chen Y, Cui Y, Wang Z, Qian G. Boosting hydrogen generation by anodic oxidation of iodide over Ni-Co $(OH)_2$ nanosheet arrays. Nanoscale Adv. 2021;3:604–610.

[15] Şahin EA, Kardaş G. Cobalt-modified nickel–zinc catalyst for electrooxidation of methanol in alkaline medium. J Solid State Electrochem. 2013;17:2871–2877.

[16] R. Ortiz, Márquez OP, Márquez J, Gutiérrez C. Necessity of oxygenated surface species for the electrooxidation of methanol on iridium. J Phys Chem B. 1996;100(20): 8389–8396.

[17] Radi AE, Ashour WFD, Elshafey R. Glycerol electrocatalytic oxidation on nickel hydroxide nanoparticles/poly-eriochrome black t modified electrode. Electrocatalysis. 2022;13:653–662.

[18] Rozario A, Silva RKSe, Freitas MBJG. Recycling of nickel from NiOOH/Ni $(OH)_2$ electrodes of spent Ni–Cd batteries. J Power Sources. 2006;158:754–759.

[19] Barakat NAM, Khalil KA, Mahmoud IH, Kanjwal MA, Sheikh FA, Kim HY. CoNi bimetallic nanofibers by electrospinning: Nickel-based soft magnetic material with improved magnetic properties. J Phys Chem C. 2010;114:15589-15593.

[20] Lima VS, Almeida TS, Andrade ARD. Glycerol electro-oxidation in alkaline medium with Pt-Fe/C electrocatalysts synthesized by the polyol method: Increased selectivity and activity provided by less expensive catalysts. Nanomater. 2023;13:1173-1190.

[21] Zalineeva A, Baranton S, Coutanceau C. How do Bi-modified palladium nanoparticles work towards glycerol electrooxidation an in situ FTIR study. Electrochim Acta. 2015;176:705-717.

[22] Jeffery DZ, Camara GA. The formation of carbon dioxide during glycerol electrooxidation in alkaline media: First spectroscopic evidences. Electrochem commun. 2010;12(8):1129-1132.

[23] Wang C-Y, Yu Z-Y, Li G, Song Q-T, Li G, Luo C-X. Intermetallic PtBi nanoplates with high catalytic activity towards electro-oxidation of formic acid and glycerol. Chem Electro Chem. 2020;7(1):239-245.

[24] Houache MSE, Hughes K, Safari R, Botton GA, Baranova EA. Modification of nickel surfaces by bismuth: Effect on electrochemical activity and selectivity toward glycerol. ACS Appl Mater Interfaces 2020;12(13):15095–15107.

[25] Coutanceau C, Baranton S, Kouamé RSB. Selective electrooxidation of glycerol into value-added chemicals: A Short Overview. Front Chem. 2019;7:1-15.

[26] Nascimento AA, Alencar eM, Zanata CR, Teixeira-Neto E, Mangini APM, Camara GA. First assessments of the influence of oxygen reduction on the glycerol electrooxidation reaction on Pt. Electrocatalysis. 2019;10:82-94.

## 9. Appendix

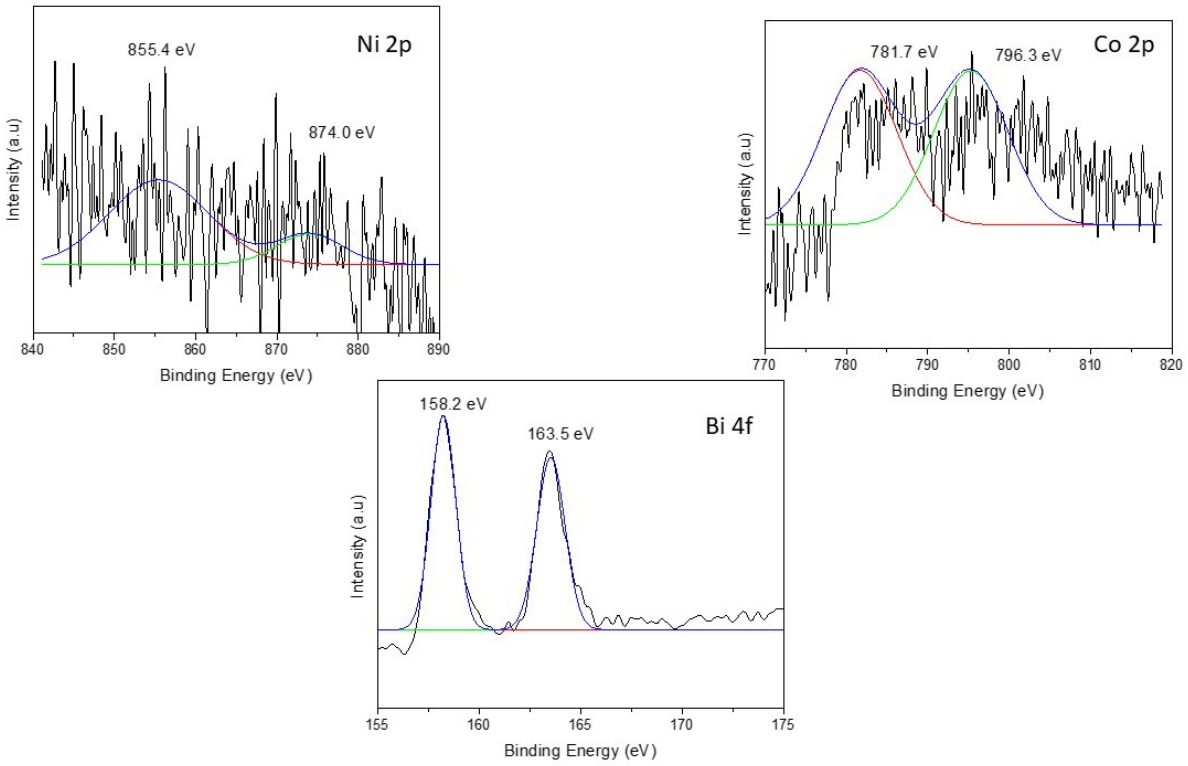


**Figure S1** XPS spectra of Ni 2*p*, Co 2*p*, and Bi 4*f* on CoNiBi_3/CC

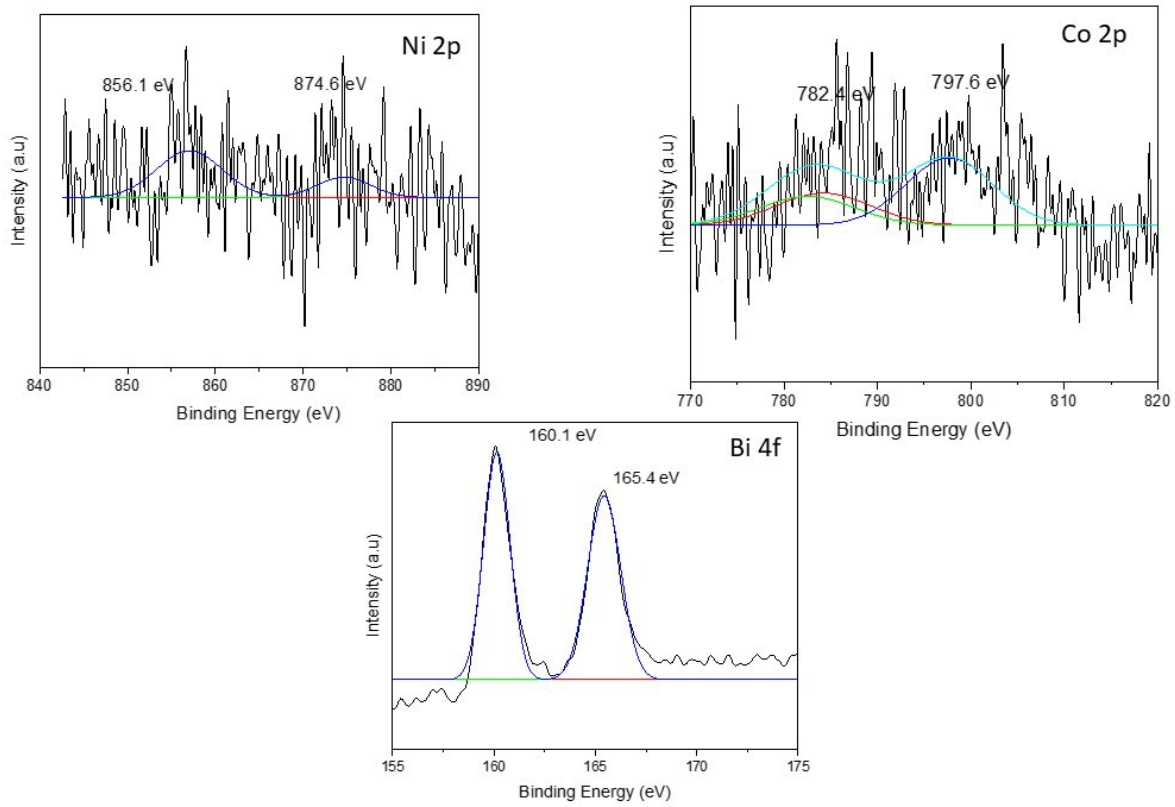


**Figure S2** XPS spectra of Ni 2*p*, Co 2*p*, and Bi 4*f* on CoNiBi_6/CC.

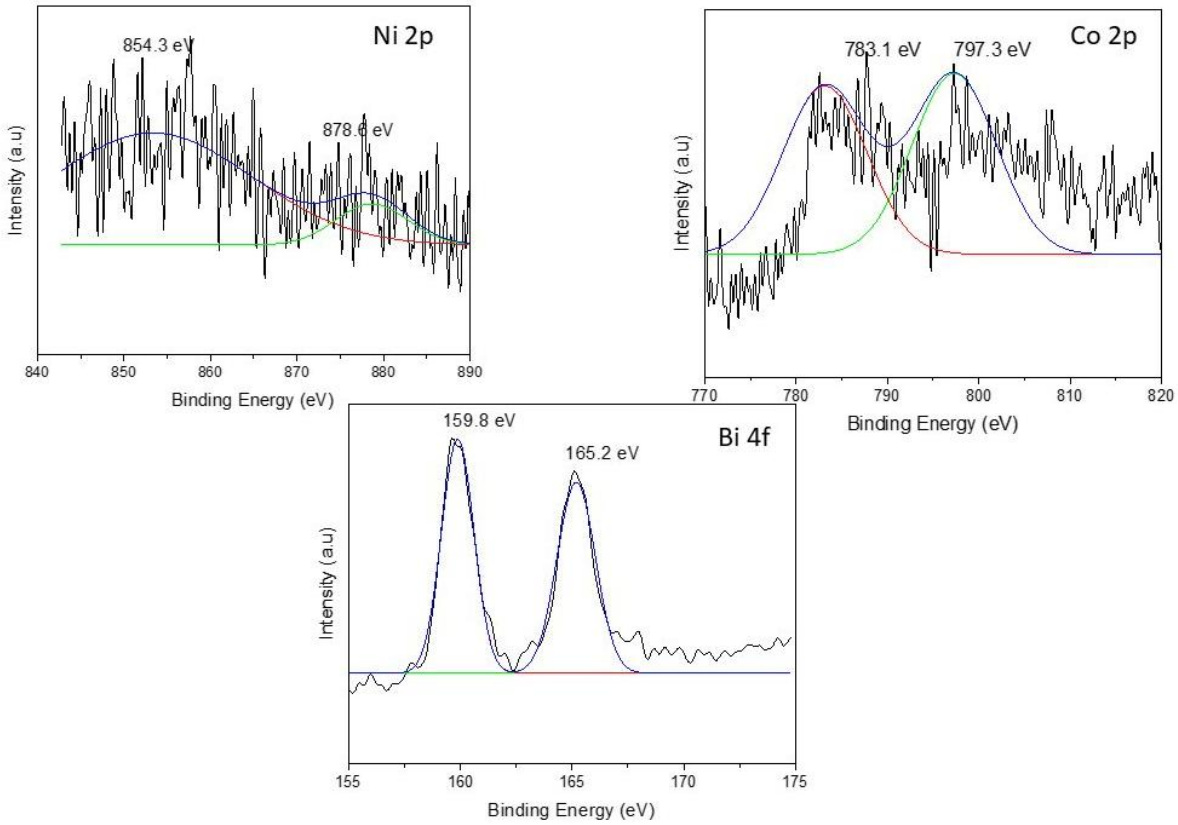


**Figure S3** XPS spectra of Ni 2*p*, Co 2*p*, and Bi 4*f* on CoNiBi_9/CC.

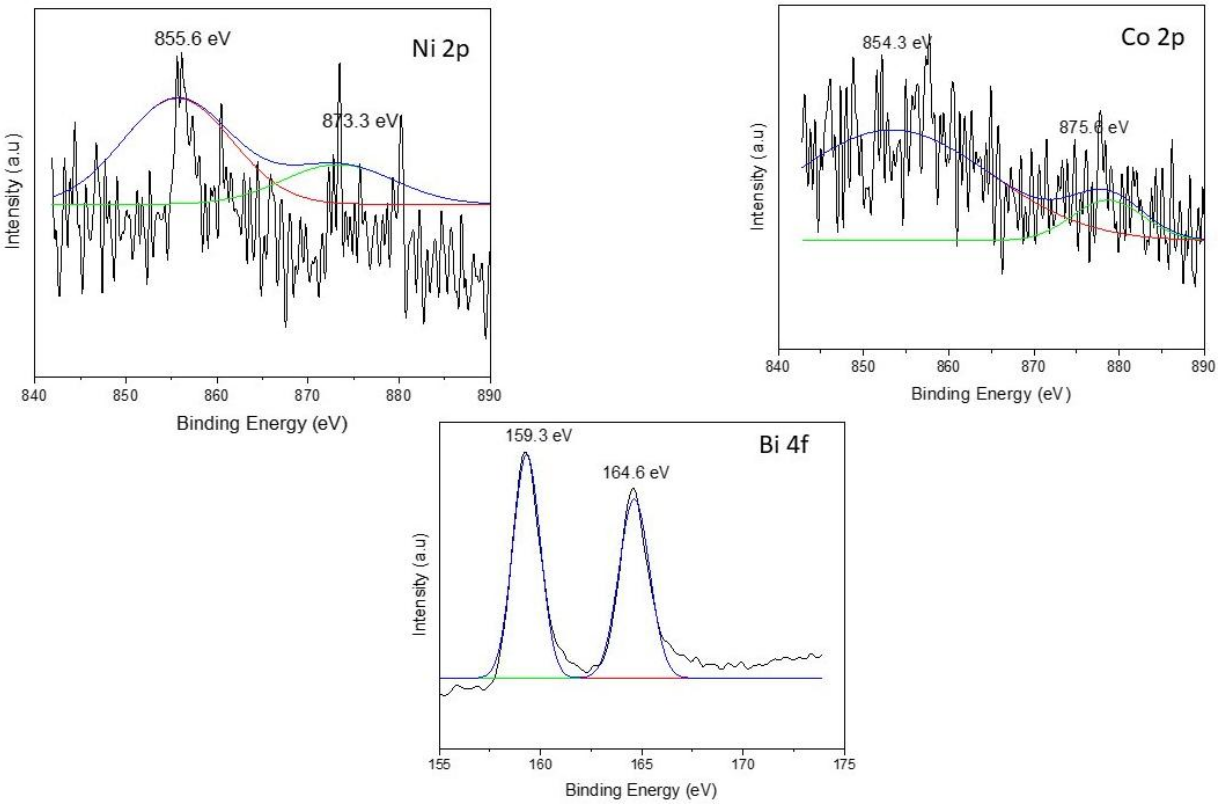


**Figure S4** XPS spectra of Ni 2*p*, Co 2*p*, and Bi 4*f* on CoNiBi_12/CC.

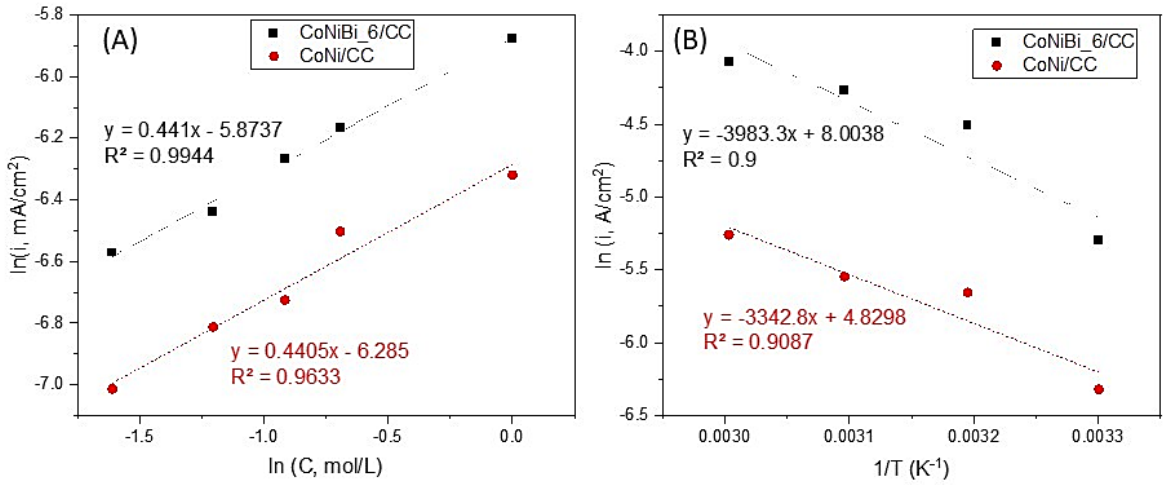


**Figure S5** Effects of (A) concentrations and (B) temperatures on EOG.

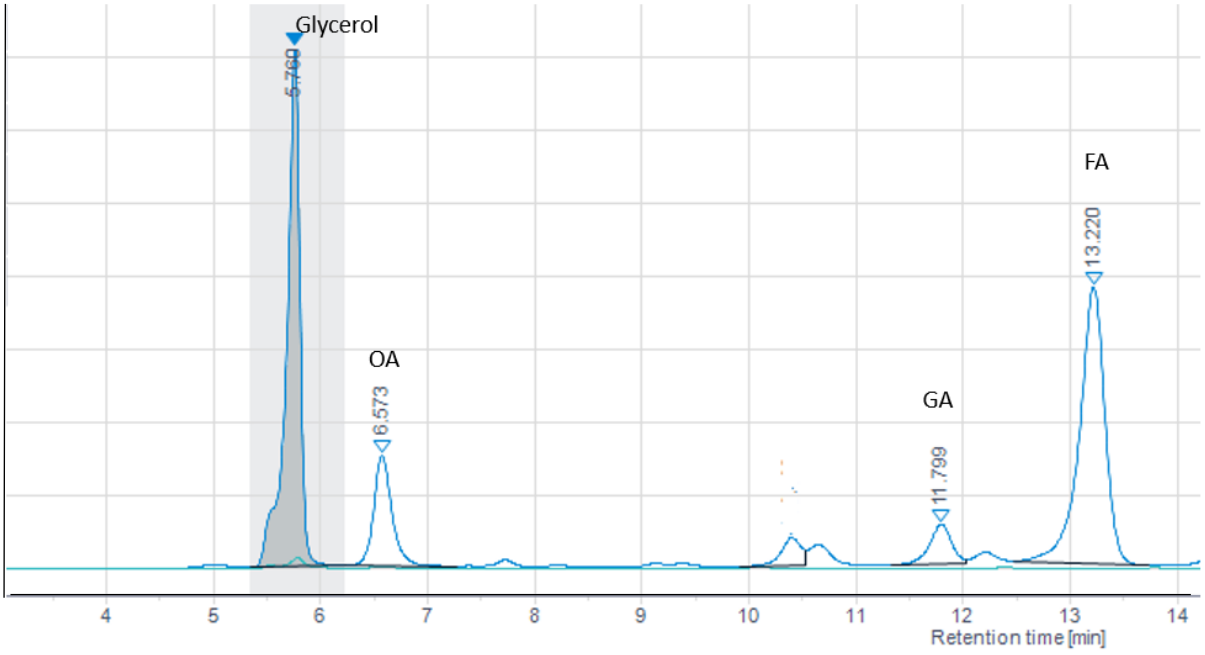


**Figure S6** Example of liquid products detected by HPLC from EOG on the CoNiBi_6/CC at 0.8 V vs Ag/AgCl.